Carbohydrate Polymers 89 (2012) 971–978

Contents lists available at SciVerse ScienceDirect

Carbohydrate Polymers

journal homepage: www.elsevier.com/locate/carbpol

Simultaneous improvement of mechanical properties and thermal stability of bacterial polyester by cellulose nanocrystals

Hou-Yong Yu, Zong-Yi Qin*, Yan-Nan Liu, Long Chen, Na Liu, Zhe Zhou*

State Key Laboratory for Modification of Chemical Fibers and Polymer Materials, and College of Materials Science and Engineering, Donghua University, Shanghai 201620, China

ARTICLE INFO

Article history:
Received 9 March 2012
Received in revised form 11 April 2012
Accepted 13 April 2012
Available online 30 April 2012

Keywords:
Poly(3-hydroxybutyrate-co-3-hydroxyvalerate)
Cellulose nanocrystal
Nanocomposite
Mechanical property
Thermal stability

ABSTRACT

Green nanocomposites were prepared by adding well-dispersed cellulose nanocrystals (CNCs) into bacterial polyester poly(3-hydroxybutyrate-co-3-hydroxyvalerate) (PHBV) matrix. Simultaneous enhancements on the mechanical property and thermal stability of PHBV after reinforcement of CNCs were achieved. Compared to neat PHBV, a 149% improvement in tensile strength and 250% increase in Young's modulus can be obtained for the resulting nanocomposites with 10 wt.% CNCs, more importantly, the T_0, $T_{5\%}$, T_{max} and T_f increased by 51.4, 36.5, 47.1 and 52.9 °C, respectively. This was due to a combination of CNCs reinforcement in the polymeric matrix, and especially the formation of strong intermolecular hydrogen bonding interactions through achieving the excellent dispersion of CNCs in the PHBV matrix via the solvent exchange procedure, as a result, the formation of six-membered ring ester during the degradation process of PHBV was clearly suppressed.

1. Introduction

Because the poorly mechanical and thermal properties of biodegradable polymers always restrict their wide applications, nanoscale reinforcements have strong promise in designing eco-friendly green nanocomposites by combining (natural/bio) fibers with biodegradable polymers (Eichhorn et al., 2010; Pei, Zhou, & Berglund, 2010; Petersson, Kvien, & Oksman, 2007; Singh, Mohanty, Sugie, Takai, & Hamada, 2008; Siqueira, Bras, & Dufresne, 2009). Cellulose nanocrystals (CNCs) with high Young's modulus (150 GPa) and strength (10 GPa) have been becoming more and more attractive as a low density reinforcing material for the nanocomposites, since the mechanical properties of polymeric matrix can be enhanced largely by introducing a small amount of the CNCs (Siqueira et al., 2009). Favier et al. first found a significant increase in the storage modulus from 0.1 MPa for neat poly(styrene-co-butyl acrylate) to 10 MPa for the nanocomposites by adding 2 wt.% CNCs (Favier, Chanzy, & Cavaillé, 1995). Similar enhancements have been continuously achieved for other biodegradable polymers, such as polycaprolactone (PCL) (Habibi & Dufresne, 2008; Habibi et al., 2008; Siqueira et al., 2009), polyvinyl alcohol (PVA) (Peresin, Habibi, Zoppe, Pawlak, & Rojas, 2010), polylactic acid (PLA) (Bondeson & Oksman, 2007; Iwatake, Nogi, & Yano, 2008; Oksman, Mathew, Bondeson, & Kvien, 2006; Pei et al., 2010; Petersson et al., 2007), plasticized starch (Anglès & Dufresne., 2001; Chen, Liu, Chang, Cao, & Anderson, 2009; Kvien, Sugiyama, Votrubec, & Oksman, 2007; Mathew & Dufresne, 2002), poly(ethyleneoxide) (Azizi Samir, Alloin, Gorecki, Sanchez, & Dufresne, 2004), and cellulose acetate butyrate (Grunert & Winter, 2002; Petersson, Mathew, & Oksman, 2009). Recently, Wolcott et al. found that tensile strength was increased from 14.1 MPa for neat PHBV to 26.1 MPa for PHBV nanocomposites with 5 wt.% CNCs by solution casting method. Moreover, they observed that the melt-processed nanocomposites exhibited lower strength than that for solution-processed nanocomposites, being ascribed to better dispersion of the CNCs in the PHBV matrix through a solution casting process (Jiang, Morelius, Zhang, Wolcott, & Holbery, 2008). Then they introduced polyethylene glycol (PEG) as a compatibilizer to improve the dispersion of CNCs in polymeric matrix, as expected, the nanocomposite exhibited a 77% improvement in Young's modulus, and 35.5% in tensile strength compared to neat PHBV (Ten, Turtle, Bahr, Jiang, & Wolcott, 2010). Unfortunately, nearly no obvious change in the degradation temperature of PHBV nanocomposites can be observed in the above-mentioned works.

The reinforcing effect of the CNCs depends on not only their nature, content and state of dispersion within the polymeric matrix, but also the intermolecular interactions between the above two components (Habibi, Lucia, & Rojas, 2010). It has been demonstrated that strong hydrogen bonding interactions occur between carbonyl groups of PHBV and hydroxyl groups in CNCs (Jiang et al., 2008; Ten et al., 2010). It is clear that good dispersion of the

* Corresponding authors. Tel.: +86 21 67792861; fax: +86 21 67792855.
E-mail addresses: phqin@dhu.edu.cn (Z.-Y. Qin), zzhe@dhu.edu.cn (Z. Zhou).

0144-8617/$ – see front matter © 2012 Elsevier Ltd. All rights reserved.
http://dx.doi.org/10.1016/j.carbpol.2012.04.053

CNCs in the polymer matrix was beneficial to form more hydrogen bonding interactions between them, being a prerequisite to achieve a maximum performance of the CNC/polymer nanocomposites (Eichhorn et al., 2010; Habibi et al., 2010; Peresin et al., 2010). Generally, the CNCs are obtained by the sulfuric acid hydrolysis of cellulose-based materials in aqueous solution, and then freeze dried in a vacuum chamber. It is very difficult to avoid the aggregation of the CNCs during nanocomposite preparation when the as-produced CNCs are dispersed into organic polymer solution again (De Menezes, Siqueira, Curvelo, & Dufresne, 2009; Eichhorn et al., 2010; Habibi et al., 2010). Although some anionic surfactants and low molecular weight esters have been successfully used to improve the dispersion of CNCs in the polymer matrix, at the same time they also caused the thermal degradation of matrix polymers (Pei et al., 2010; Petersson et al., 2007). Recently, a solvent exchange approach has been applied to obtain efficiently dispersed CNCs in organic solution of ethylene oxide-epichlorohydrin copolymer, inducing great increase in shear modulus of the nanocomposites (Capadona et al., 2007; Eichhorn et al., 2010; Habibi et al., 2010). In this work, well-dispersed CNCs in a good solvent for PHBV can be achieved by the solvent exchange approach, and a series of PHBV/CNC nanocomposites with various CNC contents were prepared. The microstructure and thermal degradation behavior of the resulting nanocomposites would be studied for understanding the underlying mechanism of the enhancement on the mechanical and thermal properties of PHBV.

2. Experimental

2.1. Materials

PHBV ($M_n = 5.90 \times 10^4$, $M_w = 1.58 \times 10^5$, and the molar ratio of HV is 2.57%) was obtained from Tiannan Biological Material Co., Ltd. (Ningbo, China) and purified by reprecipitation in methanol from chloroform solutions. Commercial microcrystalline cellulose (MCC, particle size: about 20 μm), sulfuric acid (98%), acetone (99%), chloroform (99%) and $CaCl_2$ were purchased from the Shanghai Guoyao Group Chemical Reagent Co., Ltd. (Shanghai, China). Chloroform was distilled over $CaCl_2$ before using and other reagents were used as received without further purification.

2.2. Preparation of the PHBV/CNC nanocomposites

The highly dispersed CNCs in chloroform were achieved through the solvent exchange approach as described previously (Capadona et al., 2007; Siqueira et al., 2009). MCC was firstly hydrolyzed with sulfuric acid solution of 64 wt.% at 50 °C for 1 h under strongly mechanical stirring. After cooling to room temperature, the resultant suspension was repeatedly washed by successive centrifugations (12,000 rpm at 10 °C for 20 min) with deionized water until approximate neutrality had been attained. The as-prepared CNCs were subsequently exchanged from water to acetone, then from acetone to chloroform by several successive centrifugation steps (12,000 rpm at 10 °C for 45 min). After 10 min of exposure to ultrasonic irradiation, the CNC suspension in chloroform was stored at 4 °C before using.

PHBV/CNC nanocomposites (1–20 wt.% CNCs) were prepared by gradually adding the CNC suspensions at various concentrations into chloroform solution of PHBV in ice water bath for 30 min under ultrasonic irradiation. Then the PHBV/CNC nanocomposite films with the thickness of approximately 50 μm were obtained on a glass slide through the solution casting technique. After being visibly dried, the films were further dried under vacuum at 40 °C until no obvious absorption of chloroform (754 cm^{-1}) appeared in the IR spectrum.

2.3. Characterization

The morphology of CNCs and the fracture morphologies of the nanocomposite films were observed on a field emission scanning electron microscopy (FE-SEM, HITACHI S-4800).

Tensile properties of neat PHBV and the nanocomposite films were measured on a Kexin WDW3020 electronic universal testing machine. Tensile specimens with 10 mm in width, 50 μm in thickness, and 50 mm in gauge length were loaded at a constant tensile rate of 1 mm/min, and 10 replicates were tested for each sample.

The TGA was conducted on a NETZSCH TG 209 F1 thermogravimetric analyzer from 30 to 600 °C under a dynamic nitrogen atmosphere with the flow rate of 30 mL/min and the heating rates of 10, 20, 30, and 40 °C/min, respectively. The kinetic activation energy is then determined from a plot of the logarithm of the heating rate versus the reciprocal of the temperature of constant decomposition level. Main thermal parameters were obtained from TGA curves at the heating rate of 10 °C/min, such as initial decomposition temperature (T_0), temperature at 5% weight loss ($T_{5\%}$), maximum decomposition temperature (T_{max}) and complete decomposition temperature (T_f).

The non-isothermal crystallization and melting behavior were characterized on a differential scanning calorimetry (MDSC TA-2910). The sample was firstly heated from room temperature to 200 °C at a rate of 20 °C/min, and kept at 200 °C for 5 min to eliminate the previous heat history. Subsequently, the sample was cooled to 0 °C at a rate of 10 °C/min, and heated again to 200 °C at a rate of 10 °C/min. Main thermal parameters were obtained from DSC curves, such as melt crystallization temperature (T_{mc}), melt crystallization enthalpies (ΔH_{mc}), cold crystallization temperature (T_{cc}), cold crystallization enthalpies (ΔH_{cc}), melting temperature (T_{m1}, T_{m2}), melting enthalpies (ΔH_m), the onset temperature of crystallization ($T_{c(onset)}$), the non-isothermal crystallization temperature (T_c) and width at half-height of crystallization peak (ΔW).

The crystal structures were determined on a RIGAKU D/Max-2550 PC diffractometer with an area detector operating under Cu Kα (1.5418 Å) radiation (40 kV, 40 mA). All the samples stood for 2 weeks at room temperature to reach equilibrium crystallization before using. The degree of crystallinity was taken as the ratio of the sum of areas under the crystalline diffraction peaks to the total area under the curve between $2\theta = 10^\circ$ and 60°. The chemical structures were characterized on a Nicolet 8700 Fourier transform infrared spectrometer. Each spectrum was collected with 64 scans and 2 cm^{-1} resolution.

The thermal degradation behavior was monitored on a NETZSCH TG 209 F1 thermogravimetric analyzer that was interfaced to a Nicolet 8700 Fourier transform infrared spectrometer (TG/FT-IR). The TG outlet was coupled on-line with the spectrometer through a gas cell, which was heated to 200 °C and stabilized for 4 h before the running of TG. The thermal degradation was carried out at a scan rate of 10 °C/min over a range of 30–600 °C under a nitrogen atmosphere stream with the flow rate of 30 mL/min, meanwhile the FT-IR spectra were reordered. All runs were performed in duplicate, and the infrared bands for carbon dioxide were ignored in the spectra analysis.

3. Results and discussion

3.1. Mechanical properties of PHBV/CNC nanocomposites

Fig. 1 gives the tensile strength, Young's modulus and elongation to break as a function of the CNC contents for neat PHBV and the nanocomposites. It is clear that the incorporation of CNCs in the PHBV matrix can induce an enhancement in the mechanical properties of the nanocomposites. When the CNC contents increases

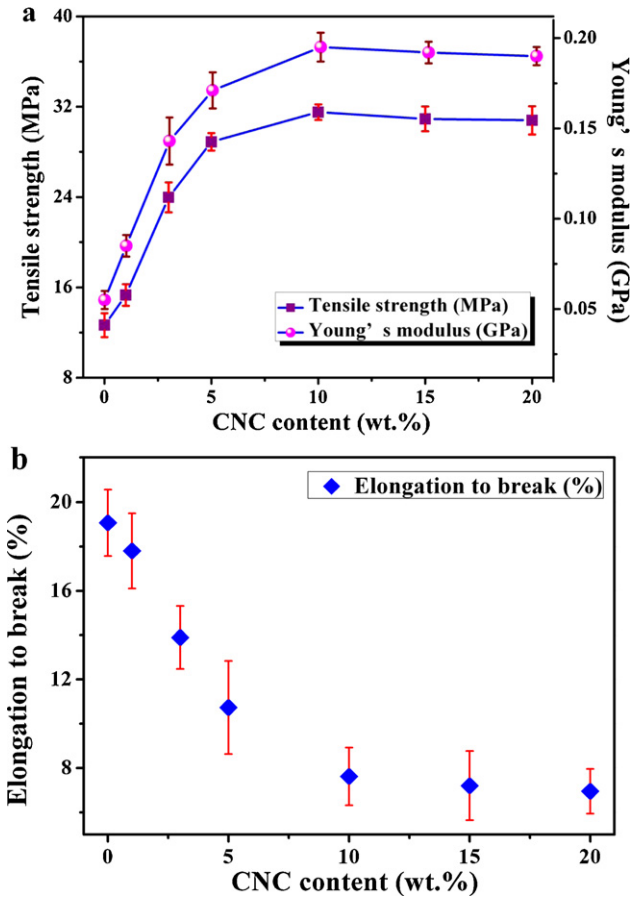

Fig. 1. Tensile strength and Young's modulus (a) and elongation to break (b) as a function of the CNC contents for neat PHBV and the nanocomposites.

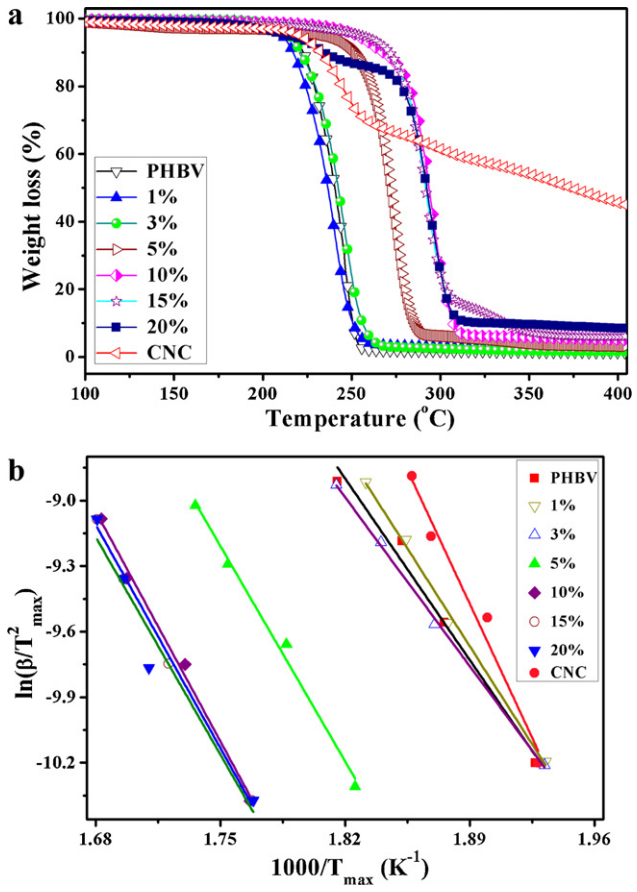

Fig. 2. TGA (a) and the plots used for the determination of the activation energies (b) for PHBV and the nanocomposites according to Kissinger's method for various CNC contents.

from 0 to 10 wt.%, the tensile strength and Young's modulus are improved dramatically by 149% and 250%, respectively, meanwhile the elongation to break reduced to 6.9%. These improvements could be attributed to the restrained chain movement during the deformation due to the presence of the CNCs, and the refined crystalline structure of PHBV after the addition of CNCs. However, once the CNC content exceeds 10 wt.%, slight decreases in the tensile strength and Young's modulus, and an increase in the elongation to break occur. On the contrary, with 5 wt.% of freeze-dried CNCs, the film showed 77% (by tensile test) improvement in Young's modulus, and 35.5% increase in tensile strength (Ten et al., 2010). Because the CNCs applied in these works are similar in size, it is believed that the aggregation of the CNCs is efficiently reduced in the preparation of nanocomposites via the solvent-exchange approach.

3.2. Thermal stability of PHBV/CNC nanocomposites

Fig. 2(a) shows the TGA curves of neat PHBV, CNCs and the nanocomposites at the heating rate of 10 °C/min, and main thermal parameters are summarized in Table 1. It is found that with the increase of the CNC contents, T_{max} gradually increases from 245.8 °C for neat PHBV to the maximum of 292.9 °C for the nanocomposite with 10 wt.% CNCs, and then decreases slightly to 292.3 °C for 20 wt.% CNCs. The similar trend can also be observed for T_0, $T_{5\%}$ and T_f. Compared with those for neat PHBV, the T_0, $T_{5\%}$, T_{max} and T_f for the nanocomposites with the best thermal stability increase by about 51.4, 36.5, 47.1 and 52.9 °C, respectively. The activation energy (E_a) can be determined using the Kissinger's equation as follows (Yeo, Tan, Bakar, & Ismail, 2010):

$$\ln \frac{\beta}{T_{max}^2} = \left\{ \ln \frac{AR}{E_a} + [n(1-\alpha_{max})^{n-1}] \right\} - \frac{E_a}{RT_{max}} \quad (1)$$

where β is the heating rate, A is the pre-exponential factor, R is the universal gas constant, α_{max} is the maximum conversion, and n is the reaction order. E_a can be calculated from the slope of $\ln(\beta/T_{max}^2)$ as a function of $1/T_{max}$ as shown in Fig. 2(b) and is listed in Table 1. With the increase of the CNC contents, E_a gradually increases from 106.3 kJ/mol for neat PHBV to the maximum 125.0 kJ/mol for the nanocomposite with 10 wt.% CNCs, and then slightly decreases. The values for all the nanocomposites are larger than 106.3 kJ/mol for neat PHBV. On the contrary, a slight increase or even decrease in the thermal stability has been reported in previous works (Bondeson & Oksman, 2007; Eichhorn et al., 2010; Fraga, Ruseckaite, & Jiménez, 2005; Habibi et al., 2010; Iwatake et al., 2008; Jiang et al., 2008; Oksman et al., 2006; Pei et al., 2010; Petersson et al., 2007; Ten et al., 2010). For example, a decrease from 295 for neat PHBV to 290 °C for the nanocomposite with 5 wt.% CNCs occurred although the dispersion of CNCs in PHBV matrix has been improved by applying PEG as a compatibilizer (Ten et al., 2010). These results indicate that the reinforcing effect depended on not only the CNCs reinforcement in the polymeric matrix, but also intermolecular hydrogen bonding interactions between the CNCs and PHBV.

3.3. Fracture morphologies of CNCs in PHBV matrix

It has been demonstrated that the solvent-exchange approach can avoid the aggregation of the CNCs in polymeric matrix

Table 1
Thermal analysis parameters, the activation energies, crystallinities and hydrogen bond fractions (F_{H-CO}) for neat PHBV and the nanocomposites with various CNC contents.

Sample	T_0 (°C)	$T_{5\%}$ (°C)[a]	T_{max} (°C)[a]	T_f (°C)[a]	E_a (kJ/mol)[b]	X_c (%)[c]	F_{H-CO}[d]
PHBV	229.4	216.8	245.8	252.3	98.7	58.1	–
1%	225.5	215.0	244.3	254.8	106.3	64.1	0.21
3%	232.8	219.9	251.3	261.4	112.1	61.8	0.24
5%	260.5	236.2	274.6	283.3	117.1	55.3	0.30
7%	268.4	241.2	283.3	294.5	121.3	55.1	0.34
10%	280.8	253.3	292.9	305.2	125.0	53.9	0.37
15%	278.8	253.0	292.5	304.5	122.2	53.1	0.37
20%	278.2	223.9	292.3	304.2	120.6	52.7	0.36
CNC	228.2	221.0	245.4	266.6	225.4	84.3	–

[a] The values of T_0 (°C), $T_{5\%}$ (°C), T_{max} (°C), T_f (°C) were obtained from the TGA curves at the heating rate of 10 °C/min.
[b] E_a was calculated from the slope of $\ln(\beta/T_{max}^2)$ as a function of $1/T_{max}$.
[c] X_c was calculated from the WAXD patterns.
[d] F_{H-CO} was obtained from the results of deconvoluted FT-IR spectra.

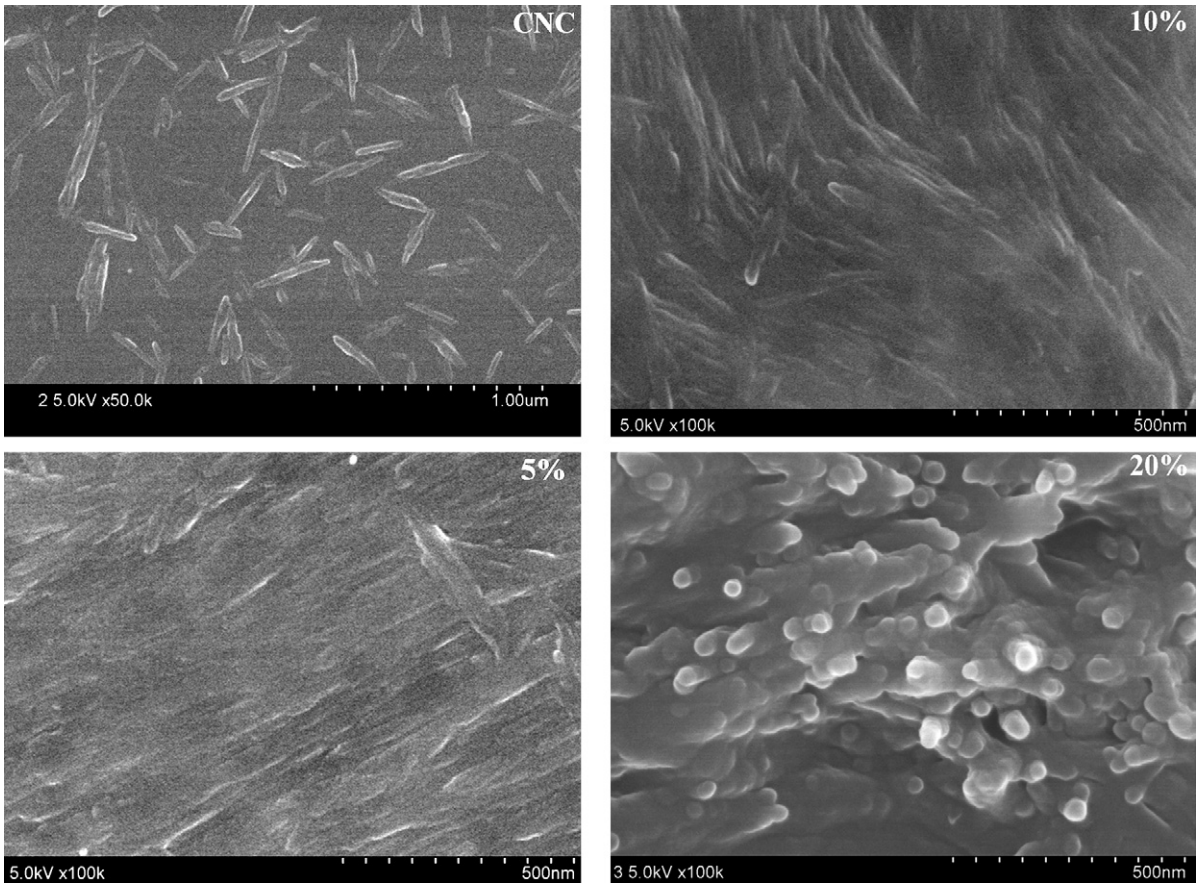

Fig. 3. FE-SEM images for the CNCs and the fracture morphologies of the nanocomposites with the CNC contents of 5, 10 and 20 wt.%.

(Capadona et al., 2007; Habibi et al., 2010). Therefore, the enhancements on the mechanical property and thermal stability of PHBV/CNC nanocomposites can be attributed to the homogenous dispersion of CNCs in the PHBV matrix through solvent exchange procedure, which can be estimated by observing the fracture morphologies of the PHBV/CNC nanocomposites. As shown in Fig. 3(a), FE-SEM shows that the used CNCs with rod-shaped morphology are about 20 nm in diameter and 230 nm in length. It is found that similar striated and smooth fractured surface can be observed for the nanocomposites with the increase of the CNC content up to 10 wt.% as shown in Fig. 3(b) and (c), indicating good dispersion of CNCs in PHBV matrix. Once the CNC content is higher than 10 wt.%, the CNCs can be in various levels of aggregation making them tens of nanometers wide or more as shown in Fig. 3(d). These observations are corresponding to the largest improvements in the mechanical and thermal properties achieved at 10 wt.% CNCs.

3.4. Non-isothermal crystallization and melting behavior of PHBV/CNC nanocomposites

The incorporation of CNCs would evidently change the crystallization and nucleation behavior of PHBV. Fig. 4 gives the first cooling (a) and second heating (b) curves of neat PHBV and the nanocomposites with various CNC contents, and the corresponding thermal parameters are listed in Table 2. As shown in Fig. 4(a), no obvious melt crystallization peaks appears for the neat PHBV and the nanocomposites with 1 wt.% CNCs during the first cooling scans, whereas the cold crystallization peak can be found in the

Table 2
Thermal parameters of non-isothermal crystallization and melting behaviors of neat PHBV and the nanocomposites with various CNC contents.

Sample	T_{mc} (°C)	ΔH_{mc} (J/g)	T_{cc} (°C)	T_{m1} (°C)	T_{m2} (°C)	ΔH_m (J/g)	$T_{c(onset)} - T_c$ (°C)	ΔW (°C)
PHBV	–	–	41.2	111.7	130.7	74.7	24.3	16.4
1%	–	–	38.8	107.2	127.7	72.3	21.4	15.1
3%	56.8	32.7	–	131.2	142.1	70.5	20.4	14.5
5%	89.9	55.8	–	147.5	156.9	66.6	16.6	9.5
10%	92.3	58.9	–	157.8	168.3	68.4	13.9	6.9
15%	91.4	53.8	–	153.3	164.5	66.9	15.4	9.2
20%	57.4	47.4	–	150.5	164.8	62.8	18.1	11.4

second heating scans. On one hand, with the increase of the CNC contents from 3 to 20 wt.%, the melt crystallization temperature (T_{mc}) first increases from 56.8 °C to a maximum value of 92.3 °C for 10 wt.% CNCs, and then gradually reduces to 57.4 °C for 20 wt.% CNCs. At the same time, the melt crystallization peaks become narrow, implying easier crystallization in the presence of the CNCs due to the lower activation energy barrier in the high-temperature region (Lin, Huang, Chang, Feng, & Yu, 2011). On the other hand, $T_{c(onset)} - T_c$ value also decreases from 24.3 °C for neat PHBV to a minimum value of 13.9 °C for 10 wt.% CNCs, and then increases to 18.1 °C for 20 wt.% CNCs. The parameter $T_{c(onset)} - T_c$ is used herein to be a measure of the overall rate of crystallization, and the smaller the $T_{c(onset)} - T_c$ is, the greater the rate of crystallization is (Li, Lai, & Liu, 2004; Liu, Zhu, Wu, & Qin, 2009). In addition, as shown in Table 2, ΔW for the nanocomposites becomes smaller than that for neat PHBV, indicating a narrower size distribution of the PHBV crystallites in the nanocomposites (Liu et al., 2009). These results reveal that the incorporation of CNCs would increase not only the nucleation rate of the nanocomposites, but also the crystallization rate, leading to a narrow distribution in the PHBV crystallite size.

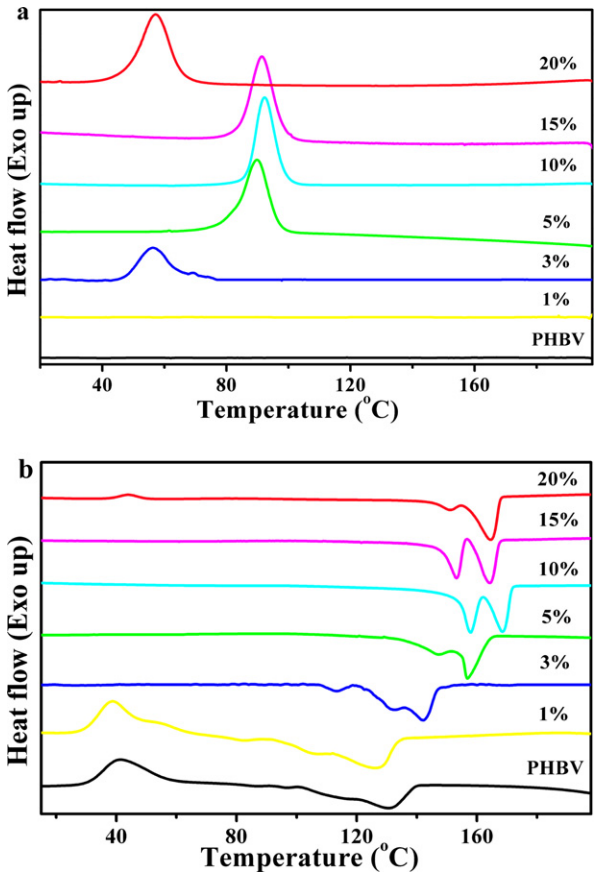

Fig. 4. DSC curves of neat PHBV and the nanocomposites with various CNC contents. (a) The first cooling scan and (b) the second heating scan.

Obvious cold crystallization peaks appear in the second heating scans for neat PHBV as shown in Fig. 4(b). With the increase of the CNC contents, the cold crystallization peak become weak together with a decrease in T_{cc}, and finally disappears once the CNC content reaches to 3 wt.%. At the same time, the melt crystallization peak appears in the nanocomposites. In the previous reports, the cold crystallization peak can be still observed for the nanocomposite with 5 wt.% CNCs, and the T_{cc} decreases by about 10 °C as compared with 51.2 °C of PHBV (Jiang et al., 2008; Ten et al., 2010). It is well known that the cold crystallization can be remarkably suppressed in the second heating scan once the nanocomposites do undergo enough crystallization in the first cooling process. This result implies that the crystallization of PHBV becomes easier in our system. Meanwhile, as shown in Fig. 4(b), a double melting peak appeared during melting–recrystallization–melting process becomes stronger for the nanocomposite compared with that for neat PHBV. Table 2 clearly shows that with the increase of the CNC contents, T_{m2} increases from 130.7 for neat PHBV to a maximum value of 168.3 °C for 10 wt.%, and then slightly decreases to 164.8 °C for 20 wt.%. Generally, the higher T_{m2} is, the higher perfection and thicker lamellar layers of PHBV crystals are (Jiang et al., 2008; Liu et al., 2009; Ten et al., 2010). The results evidently support that the nucleation capability and crystallization rate of neat PHBV can be greatly enhanced by achieving homogeneous incorporation of CNCs in polymeric matrix.

3.5. Crystal structure and crystallinity of PHBV/CNC nanocomposites

The physical properties of the nanocomposites depend on not only the strength of the intermolecular forces, but also the change in the crystallinity of PHBV. The crystal structures of neat PHBV, CNCs and the nanocomposites were studied by WAXD patterns, and calculated crystallinities (X_c) are given in Table 1. The CNCs exhibit typical pattern of cellulose I diffractogram and cannot be clearly identified in the patterns of the nanocomposites even for 20 wt.% CNCs. All the nanocomposites show a similar diffraction pattern, but the X_c increases from 58.1 for neat PHBV to a maximum value of 64.1% for the nanocomposite with 1 wt.% CNCs, and decreases gradually to 52.7% for the nanocomposite with 20 wt.% CNCs. It reveals that CNCs are the most efficient nucleation agent to promote the crystallization rate, however, but not the crystallinity (Ten et al., 2010). The CNCs can affect the crystallization of PHBV in two opposite ways. On one hand, the CNCs can act as a nucleating agent in the PHBV matrix, which increase the nucleation and the overall crystallization rate, leading to more perfect PHBV crystals. On the other hand, owing to the strong interactions between the CNCs and PHBV, the motion of the PHBV chains is restricted and subsequently the crystallinity decreases. Therefore, the crystallization rate increases with the increase of the CNC contents, whereas the crystallinity decreases under good dispersion conditions. A similar phenomenon has been noted in the acetylated cellulose nanocrystals/poly(lactic acid) nanocomposites (Lin et al., 2011).

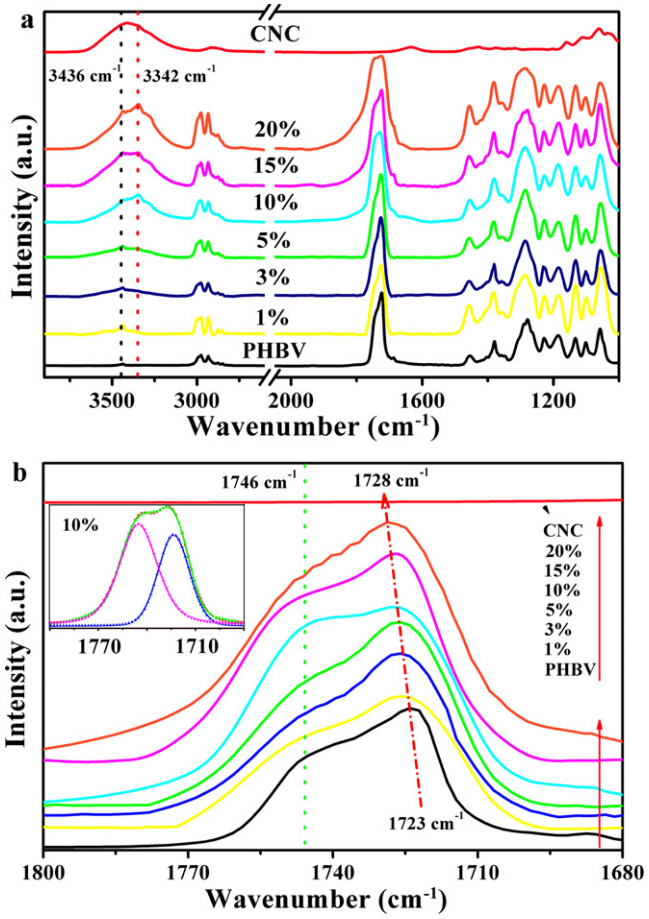

Fig. 5. FT-IR spectra (a) and carbonyl stretching region ($\nu_{C=O}$) in the infrared spectra (b) for the nanocomposites with various CNC contents and peak deconvolution for the nanocomposites with 10 wt.% CNCs (insert).

3.6. Intermolecular hydrogen bonding interaction of PHBV/CNC nanocomposites

The influence of CNCs in the crystallinity is further investigated by deconvolution and curve fitting for FT-IR spectra of the nanocomposites. Fig. 5(a) illustrates FT-IR spectra and carbonyl stretching region ($\nu_{C=O}$) in the infrared spectra for the nanocomposites with various CNC contents. All the characteristic bands of PHBV and CNCs appear in the FT-IR spectra of the nanocomposites. Two typical O—H stretching bands (3342 and 3436 cm^{-1}) from intra- and intermolecular hydrogen bonds appear at two side of a broad band (3410 cm^{-1}) for CNCs, and these shoulders are to be ascribed to the stretching vibrations of the hydrogen bonded and free O—H groups, respectively (Fei et al., 2003; Hameed, Guo, Tay, & Kazarian, 2011; Peresin et al., 2010; Suttiwijitpukdee, Sato, Zhang, Hashimoto, & Ozaki, 2011). With the increase of the CNC contents, the intensity for low-frequency band increases, whereas for the high-frequency band slightly decreases. It shows that no new chemical bonds appear, but the strong hydrogen bonding does occur in the nanocomposites.

To determine the hydrogen bond fraction (F_{H-CO}), IR spectra of the carbonyl band in the range from 1680 to 1800 cm^{-1} were curve-fitted using Gauss/Lorentz spectral function. As shown by the insert presented in Fig. 5(b), the band situated at around 1728 cm^{-1} can be assigned to the hydrogen bonded C=O groups, and 1746 cm^{-1} to free C=O groups (Cheng, Sun, Chen, & Jean, 2009; Fei et al., 2003; Liu et al., 2009; Singh et al., 2008; Suttiwijitpukdee et al., 2011; Yoshie, Asaka, Yazawa, Kuroda, & Inoue, 2003). With the increase of the CNC contents, the band position for hydrogen-bonded component gradually shifts from 1723 cm^{-1} for neat PHBV to 1728 cm^{-1} for the nanocomposites with 20 wt.% CNCs, whereas that for free component is almost unchanged. However, the total area of the carbonyl bands becomes larger, and the fraction of free component slightly increases. Because no absorption band of the CNCs appears in this region, any change here should be directly attributed to changes in the carbonyl group environments of PHBV, such as formation of hydrogen bonds. The F_{H-CO} values can be calculated by the following equation (Hameed et al., 2011; Salim, Hameed, & Guo, 2009; Salim, Hanley, & Guo, 2010):

$$F_{H-CO} = \frac{A_H/r_{H/a}}{(A_H/r_{H/a} + A_a)} = \frac{A_H}{(A_H + r_{H/a}A_a)} \quad (2)$$

where A_a and A_H are the peak areas of free and hydrogen bonded component, respectively, and $r_{H/a}$ is the specific absorption ratio of the above two bands. For semi-quantitative comparison purposes, $r_{H/a}$ should be within a range from 1.2 to 1.75, depending on the strength of the hydrogen bonds. Herein a minimal error would be obtained using 1.32 of $r_{H/a}$, being close to 1.40 applied for PHBV/bisphenol A composites (Fei et al., 2003). Table 1 lists the F_{H-CO} as a function of the CNC contents. With the increase of the CNC contents, F_{H-CO} firstly increases from 0.21 for the nanocomposite with 1 wt.% CNCs to a maximum value of 0.37 for 10 wt.%, and then slightly decreases to 0.36 for 20 wt.%. From above, it is clearly seen that among all the nanocomposites, the strongest intermolecular interaction appears for the nanocomposite with 10 wt.% CNCs, as a result, the largest improvements in the mechanical and thermal properties can be achieved.

3.7. Thermal degradation of PHBV/CNC nanocomposites

To understand the underlying mechanism of the enhancement in thermal stability of PHBV nanocomposites, their thermal degradation processes were monitored by TG/FT-IR. Fig. 6 shows the stack plots of TG/FT-IR for neat PHBV and the nanocomposite with 10 wt.% CNCs. Similar infrared bands can be observed for neat PHBV and the nanocomposite, indicating almost same products formed in the thermal decomposition of PHBV. The results imply that the main decomposition pathway of PHBV do not seem to be affected by introducing CNCs, but the temperature for producing the detectable volatile products increases from 246.2 °C for neat PHBV to a maximum of 299.5 °C for the nanocomposite with 10 wt.% CNCs. Further, the shorter time required for the total degradation, or narrower degradation temperature range for the PHBV nanocomposite is observed compared with neat PHBV. The total degradation took placed within a temperature range from 225.0 to 600.0 °C for neat PHBV, whereas from 270.0 to 500.0 °C for the nanocomposite with 10 wt.% CNCs. These results illustrate that some specific conformational changes of PHBV in the early stage of thermal degradation (see insert of Fig. 6(a)) are delayed by incorporating CNCs, but the total decomposition process is greatly accelerated after the maximum degradation temperature. It is widely accepted that the chain scission of PHBV molecules during thermal degradation progresses by a random cis-elimination reaction at a six-membered ring ester intermediate (Cheng et al., 2009; Li, Hem, Yu, & Cheung, 2003; Liu et al., 2009). For neat PHBV, as shown in Fig. 6(a), once the temperature increases to 210 °C, strong infrared absorption bands appear, such as the C=C stretching vibration band (1660 cm^{-1}), C=O stretching vibration bands (1759 and 1768 cm^{-1}), and O—H vibration bands (969 and 3583 cm^{-1}). The IR spectra indicate that likely degradation products of PHBV include unsaturated carboxyl acid and unsaturated ester (Li et al., 2003). For the nanocomposite, only weak C=O stretching bands without obvious O—H bands appear in Fig. 6(b) even if the temperature is raised up to 275 °C. It

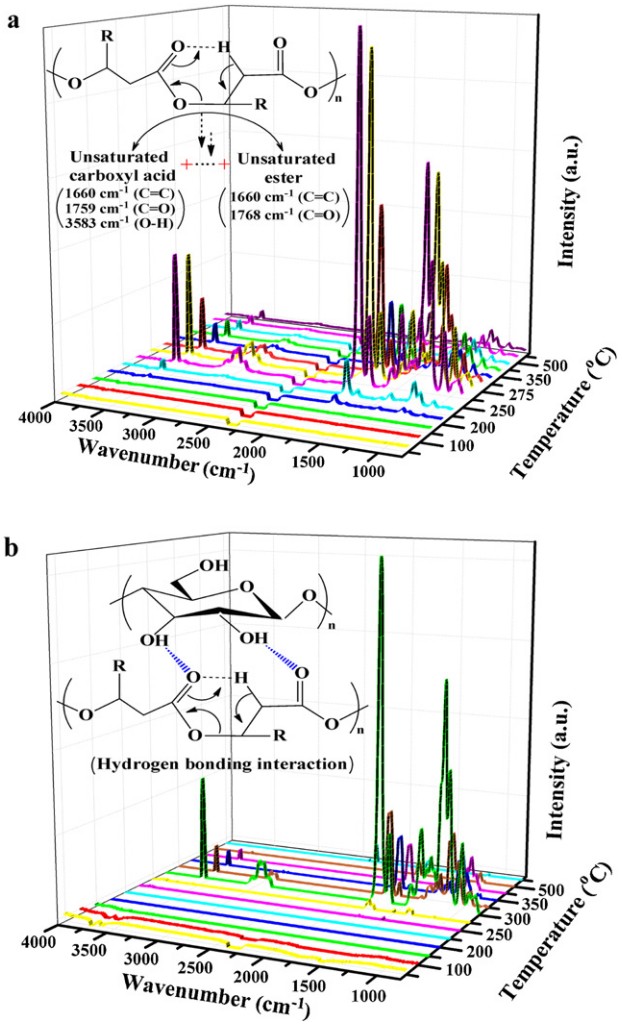

Fig. 6. TG/FT-IR stack plots for neat PHBV (a) and the nanocomposite with 10 wt.% CNCs (b).

is believed that in the early stages of decomposition of PHBV, the formation of six-membered ring ester during the degradation process of PHBV was clearly suppressed due to strong intermolecular hydrogen bonding interactions (see insert of Fig. 6(b)). However, once the temperature exceeds 300 °C, the hydrogen bonds would be broken. Strong infrared bands corresponding to carbonyl and hydroxyl stretching can be observed over relatively narrow temperature spans, indicating an accelerated degradation due to the presence of the CNCs with high thermal conductivity (Ten et al., 2010).

4. Conclusions

The green nanocomposites were successfully prepared by homogeneously incorporating various contents of CNCs into PHBV matrix. Simultaneous enhancements on the mechanical property and thermal stability of the nanocomposites were achieved. Compared with those of PHBV, the 149% improvement in tensile strength and 250% increase in Young's modulus can be obtained for the nanocomposites with 10 wt.% CNCs, meanwhile the T_0, $T_{5\%}$, T_{max} and T_f increased by 51.4, 36.5, 47.1 and 52.9 °C, respectively. Such the reinforcing effect can be attributed to high modulus and high strength of the CNCs as nanoscale reinforcement, good crystallization properties, and most importantly strong intermolecular hydrogen bonding interactions induced by achieving the excellent dispersions of CNCs in the PHBV matrix via solvent exchange procedure. The result of this study will have an important impact on broadening the practical use and understanding the thermal degradation behavior of such nanocomposites to optimize the processing conditions and their final properties.

Acknowledgments

This work was supported by the key basic research foundation of the Committee of Science and Technology of Shanghai Municipality (Grant No.: 06JC22003), the Fundamental Research Funds for the Central Universities, and the Doctorate Innovation Foundation of Donghua University (BC201101).

References

Anglès, M., & Dufresne, A. (2001). Plasticized starch/tunicin whiskers nanocomposite materials. 2. Mechanical behavior. *Macromolecules*, *34*, 2921–2931.
Azizi Samir, M. A. S., Alloin, F., Gorecki, W., Sanchez, J. Y., & Dufresne, A. (2004). Cellulose nanocrystals reinforced poly(oxyethylene). *Polymer*, *45*, 4149–4157.
Bondeson, D., & Oksman, K. (2007). Polylactic acid/cellulose whisker nanocomposites modified by polyvinyl alcohol. *Composites Part A*, *38*, 2486–2492.
Capadona, J. R., Bergm, D. O. V., Capadona, L. A., Schroeter, M., Rowan, S. J., Tyler, D. J., et al. (2007). A versatile approach for the processing of polymer nanocomposites with self-assembled nanofibre templates. *Nature Nanotechnology*, *2*, 765–769.
Chen, Y., Liu, C., Chang, P., Cao, X., & Anderson, D. (2009). Bionanocomposites based on pea starch and cellulose nanowhiskers hydrolyzed from pea hull fibre: Effect of hydrolysis time. *Carbohydrate Polymers*, *76*, 607–615.
Cheng, M. L., Sun, Y. M., Chen, H., & Jean, Y. C. (2009). Change of structure and free volume properties of semi-crystalline poly(3-hydroxybutyrate-co-3-hydroxyvalerate) during thermal treatments by positron annihilation lifetime. *Polymer*, *50*, 1957–1964.
De Menezes, A. J., Siqueira, G., Curvelo, A. A. S., & Dufresne, A. (2009). Extrusion and characterization of functionalized cellulose whiskers reinforced polyethylene nanocomposites. *Polymer*, *50*, 4552–4563.
Eichhorn, S. J., Dufresne, A., Aranguren, M., Marcovich, N. E., Capadona, J. R., Rowan, S. J., et al. (2010). Review: Current international research into cellulose nanofibres and nanocomposites. *Journal of Materials Science*, *45*, 1–33.
Favier, V., Chanzy, H., & Cavaillé, J. Y. (1995). Polymer nanocomposites reinforced by cellulose whiskers. *Macromolecules*, *28*, 6365–6367.
Fei, B., Chen, C., Wu, H., Peng, S., Wang, X., & Dong, L. (2003). Quantitative FTIR study of PHBV/bisphenol A blends. *European Polymer Journal*, *39*, 1939–1946.
Fraga, A., Ruseckaite, R., & Jiménez, A. (2005). Thermal degradation and pyrolysis of mixtures based on poly(3-hydroxybutyrate-8%-3-hydroxyvalerate) and cellulose derivatives. *Polymer Testing*, *24*, 526–534.
Grunert, M., & Winter, W. T. (2002). Nanocomposites of cellulose acetate butyrate reinforced with cellulose nanocrystals. *Journal of Polymers and the Environment*, *10*, 27–30.
Habibi, Y., & Dufresne, A. (2008). Highly filled bionanocomposites from functionalized polysaccharide nanocrystals. *Biomacromolecules*, *9*, 1974–1980.
Habibi, Y., Goffin, A. L., Schiltz, N., Duquesne, E., Dubois, P., & Dufresne, A. (2008). Bionanocomposites based on poly(ε-caprolactone)-grafted cellulose nanocrystals by ring opening polymerization. *Journal of Materials Chemistry*, *18*, 5002–5010.
Habibi, Y., Lucia, L. A., & Rojas, O. J. (2010). Cellulose nanocrystals: Chemistry, self-assembly, and applications. *Chemical Reviews*, *110*, 3315–3336.
Hameed, N., Guo, Q., Tay, F. H., & Kazarian, S. G. (2011). Blends of cellulose and poly(3-hydroxybutyrate-co-3-hydroxyvalerate) prepared from the ionic liquid 1-butyl-3-methylimidazolium chloride. *Carbohydrate Polymers*, *86*, 94–104.
Iwatake, A., Nogi, M., & Yano, H. (2008). Cellulose nanofiber-reinforced polylactic acid. *Composites Science and Technology*, *68*, 2103–2106.
Jiang, L., Morelius, E., Zhang, J., Wolcott, M., & Holbery, J. (2008). Study of the poly(3-hydroxybutyrate-co-3-hydroxyvalerate)/cellulose nanowhisker composites prepared by solution casting and melt processing. *Journal of Composite Materials*, *42*, 2629–2645.
Kvien, I., Sugiyama, J., Votrubec, M., & Oksman, K. (2007). Characterization of starch based nanocomposites. *Journal of Materials Science*, *42*, 8163–8171.
Li, S. D., Hem, J. D., Yu, P., & Cheung, M. K. (2003). Thermal degradation of poly(3-hydroxybutyrate) and poly(3-hydroxybutyrate-co-3-hydroxyvalerate) as studied by TG, TG-FTIR, and Py-GC/MS. *Journal of Applied Polymer Science*, *89*, 1530–1536.
Li, J., Lai, F., & Liu, J. J. (2004). Effect of poly(propylene carbonate) on the crystallization and melting behavior of poly(β-hydroxybutyrate-co-β-hydroxyvalerate). *Journal of Applied Polymer Science*, *92*, 2514–2521.
Lin, N., Huang, Jin., Chang, P. R., Feng, J., & Yu, J. (2011). Surface acetylation of cellulose nanocrystal and its reinforcing function in poly(lactic acid). *Carbohydrate Polymers*, *83*, 1834–1842.
Liu, Q. S., Zhu, M. F., Wu, W. H., & Qin, Z. Y. (2009). Reducing the formation of six-membered ring ester during thermal degradation of biodegradable PHBV to enhance its thermal stability. *Polymer Degradation and Stability*, *94*, 18–24.
Mathew, A., & Dufresne, A. (2002). Highly filled bionanocomposites from functionalized polysaccharide nanocrystals. *Biomacromolecules*, *3*, 609–617.

Oksman, K., Mathew, A., Bondeson, D., & Kvien, I. (2006). Manufacturing process of cellulose whiskers/polylactic acid nanocomposites. *Composites Science and Technology*, *66*, 2776–2784.

Pei, A., Zhou, Q., & Berglund, L. A. (2010). Functionalized cellulose nanocrystals as biobased nucleation agents in poly(L-lactide) (PLLA) – Crystallization and mechanical property effects. *Composites Science and Technology*, *70*, 815–821.

Peresin, M. S., Habibi, Y., Zoppe, J. O., Pawlak, J. J., & Rojas, O. J. (2010). Nanofiber composites of polyvinyl alcohol and cellulose nanocrystals: Manufacture and characterization. *Biomacromolecules*, *11*, 674–681.

Petersson, L., Kvien, I., & Oksman, K. (2007). Structure and thermal properties of poly(lactic acid)/cellulose whiskers nanocomposite materials. *Composites Science and Technology*, *67*, 2535–2544.

Petersson, L., Mathew, A. P., & Oksman, K. (2009). Dispersion and properties of cellulose nanowhiskers and layered silicates in cellulose acetate butyrate nanocomposites. *Journal of Applied Polymer Science*, *112*, 2001–2009.

Salim, N. V., Hameed, N., & Guo, Q. (2009). Competitive hydrogen bonding and self assembly in poly(2-vinyl pyridine)-block-poly(methyl methacrylate)/poly(hydroxyether of bisphenol A) blends. *Journal of Polymer Science Part B: Polymer Physics*, *47*, 1894–1905.

Salim, N. V., Hanley, T., & Guo, Q. (2010). Microphase separation through competitive hydrogen bonding in double crystalline diblock copolymer/homopolymer blends. *Macromolecules*, *43*, 7695–7704.

Singh, S., Mohanty, A. K., Sugie, T., Takai, Y., & Hamada, H. (2008). Renewable resource based biocomposites from natural fiber and polyhydroxybutyrate-co-valerate (PHBV) bioplastic. *Composites Part A*, *39*, 875–886.

Siqueira, G., Bras, J., & Dufresne, A. (2009). Cellulose whiskers versus microfibrils: Influence of the nature of the nanoparticle and its surface functionalization on the thermal and mechanical properties of nanocomposites. *Biomacromolecules*, *10*, 425–432.

Suttiwijitpukdee, N., Sato, H., Zhang, J., Hashimoto, T., & Ozaki, Y. (2011). Intermolecular interactions and crystallization behaviors of biodegradable polymer blends between poly (3-hydroxybutyrate) and cellulose acetate butyrate studied by DSC, FT-IR, and WAXD. *Polymer*, *52*, 461–471.

Ten, E., Turtle, J., Bahr, D., Jiang, L., & Wolcott, M. (2010). Thermal and mechanical properties of poly(3-hydroxybutyrate-co-3-hydroxyvalerate)/cellulose nanowhiskers composites. *Polymer*, *51*, 2652–2660.

Yeo, S. Y., Tan, W. L., Bakar, A. M., & Ismail, J. (2010). Silver sulfide/poly(3-hydroxybutyrate) nanocomposites: Thermal stability and kinetic analysis of thermal degradation. *Polymer Degradation and Stability*, *95*, 1299–1304.

Yoshie, N., Asaka, A., Yazawa, K., Kuroda, Y., & Inoue, Y. (2003). In situ FTIR microscope study on crystallization of crystalline/crystalline polymer blends of bacterial copolyesters. *Polymer*, *44*, 7405–7412.